Letter

Robust polaritons in magnetic monolayers of CrI_3

Yaroslav Zhumagulov,[1,*] Salvatore Chiavazzo,[2] Ivan A. Shelykh,[3,4] and Oleksandr Kyriienko[2]
[1]*HSE University, Moscow 101000, Russia*
[2]*Department of Physics and Astronomy, University of Exeter, Stocker Road, Exeter EX4 4QL, United Kingdom*
[3]*Science Institute, University of Iceland, Dunhagi-3, IS-107 Reykjavik, Iceland*
[4]*Department of Physics and Engineering, ITMO University, St. Petersburg 197101, Russia*

(Received 11 February 2023; revised 9 August 2023; accepted 14 August 2023; published 5 October 2023)

We show that the regime of strong light-matter coupling with remarkable magnetic properties can be implemented in systems based on monolayers of chromium triiodide (CrI_3). This two-dimensional material combines the presence of strongly bound excitonic complexes with ferromagnetic ordering below the Curie temperature. Using microscopic first-principles calculations, we reveal a rich spectrum of optical transitions corresponding to both Wannier- and Frenkel-type excitons, including those containing electrons with an effective negative mass. We show that excitons of different polarizations efficiently hybridize with a photonic mode of a planar microcavity. Due to the peculiar selection rules, polariton modes become well resolved in circular polarizations. The strong optical oscillator strength of excitons and cavity confinement leads to large values of the Rabi splitting, reaching 35 meV for a single monolayer and giant Zeeman splitting between polariton modes of up to 20 meV. This makes CrI_3 an excellent platform for magnetopolaritonic applications.

DOI: 10.1103/PhysRevB.108.L161402

Introduction. Ensembles of cavity polaritons—composite particles appearing in the regime of strong light-matter coupling—can form quantum fluids of light in optical microcavities. They represent a unique platform for studying collective quantum phenomena at surprisingly high temperatures [1]. The essential characteristic that defines the robustness of polaritonic response is a Rabi splitting Ω [2]. This parameter is defined by the cavity geometry (e.g., mode volume) and optical oscillator strength of material excitations participating in polariton formation. For Wannier-Mott excitons in GaAs samples, where the strong coupling was observed for the first time [3], the value of Ω does not exceed a few meV. Therefore, while the technology for producing high-quality GaAs samples is well developed and III-V polaritons demonstrate excellent properties at cryogenic temperatures, they do not allow room-temperature operation. The search for alternative materials with higher values of Ω is thus an actual task. Among perspective candidates, one should mention wideband semiconductors, such as GaN and ZnO [4–6], organic materials [7–12], perovskites [13–17], and carbon nanotubes [18–20].

An attractive solution is represented by monolayers of transition metal dichalcogenides (TMDs) [21], with typical examples being MoS_2, $MoSe_2$, WS_2, and WSe_2. Their two-dimensional (2D) nature, reduced screening, and relatively high effective masses of carriers lead to a substantial increase of exciton binding energy and optical oscillator strength [22]. This results in a possibility of boosting the values of Ω to tens of meV [23–28]. Paired with exciton stability, this makes polaritons robust even at room temperatures [21,29,30].

Recently, another class of 2D materials with a robust excitonic response, chromium trihalides (CrI_3 and $CrBr_3$), was discovered. Compared to typical TMD materials, they have even higher excitonic binding energies, and oscillator strengths [31] due to the specific type of excitons, which are mostly Frenkel type. As excitonic oscillator strength is proportional to the exciton confinement and dipole moment of the optical transition [32], we expect to see the enhancement of the light-matter coupling in these materials. In particular, large oscillator strengths allow to get Rabi splittings as huge as several tens of meV (see our results).

Moreover, an interesting twist is added by the magnetic nature of these, and other van der Waals (vdW) materials [33–38]. It strongly affects their transport and optical properties, leading to such phenomena as the anomalous Hall effect in CrI_3 heterostructures [39], spin-polarized optical conductivity [40], giant Kerr rotation [35], magnetic circular dichroism [41], the onset of 2D magnetoplasmons [42], and topological excitations [33].

In this Letter, we analyze the perspectives of the polaritonic applications for chromium trihalide monolayers (taking CrI_3 as an example, see Fig. 1). Focusing on the monolayer case allows us to demonstrate the excitonic Rabi splittings of several tens of meV. Even though excitons have been proven to be equally stable in multilayer and bulk samples, bulk excitons demonstrate a reduced magneto-optical response [31], thus featuring monolayers as better candidates for optical applications. Combined with giant values of excitonic Zeeman splitting stemming from the ferromagnetic ordering [43], this can be of particular importance for the observation of polariton topological phases [44–47], the polaritonic spin Meissner effect [48,49], and valleytronics [50]. Recent results on the observation of strong coupling in bulk vdW antiferromagnets

*iaroslav.zhumagulov@ur.de

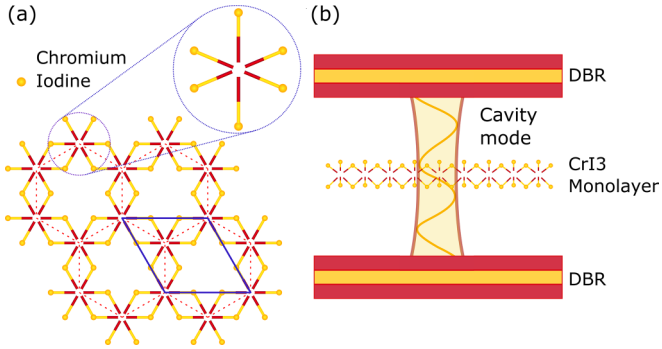

FIG. 1. (a) CrI_3 monolayer structure. Red and yellow spheres are chromium and iodine atoms. The blue parallelogram and red dashed hexagons highlight unit cells. We enlarge and show a three-dimensional visualization of a lattice site, with Cr being in the center, and six iodine atoms surrounding it (shared with other sites). (b) Polaritonic setup where a CrI_3 monolayer placed in an optical cavity enters the strong light-matter coupling regime. The optical cavity can be formed by a pair of distributed Bragg reflectors (DBRs) or a distributed Bragg reflector (bottom) and a fiber-based mirror (top).

of $NiPS_3$ show that magnetopolaritonics is well within reach of modern experiments [51].

We consider the configuration sketched in Fig. 1(b), where a CrI_3 layer is embedded in a planar microcavity. We first address the electron-hole interaction problem and solve the Bethe-Salpeter equation for the spin-resolved interaction Hamiltonian. We reveal four major energy transitions determining the relevant peaks in photoluminescence. Using the Green's function approach, we then consider the coupling between excitons and cavity photons and simulate the polaritonic spectra. We demonstrate that due to the peculiar optical selection rules and ferromagnetic properties of the CrI_3 lattice, the polaritonic modes reveal giant splitting in circular polarization.

Excitons in CrI_3 *monolayers.* We start by analyzing the properties of the bound states of electron-hole pairs in CrI_3 monolayers. The structure of the crystalline lattice of this material is schematically shown in Fig. 1(a). We calculated the exciton spectrum for a freestanding ferromagnetic CrI_3 monolayer using the numerical solution of the Bethe-Salpeter equation parametrized from the density functional theory (DFT) calculations [52].

The results are presented in Fig. 2. The full absorption profile of a CrI_3 sample is presented in Fig. 2(a). The corresponding dipole transition matrix elements are shown in Fig. 2(b). The spectrum is resolved in circular polarizations of light, and reveals pronounced nonequivalence between the σ^+ and σ^- components. Both σ^+ and σ^- profiles in Fig. 2(a) have strong absorption peaks associated with low-lying Frenkel- and Wannier-type excitons. The presence of both types of excitons have been reported in previous works [31,53]. For the σ_+ polarization, we notice the major transition at 1.7 eV, while for the σ_- polarized radiation the dominant peak is located around 1.9 eV.

Figure 2(b) presents the exciton dipole moment distribution in the sample. The optical dipole moments range from below 0.01 to 1.0 Å, for both σ_+ and σ_- polarizations. In

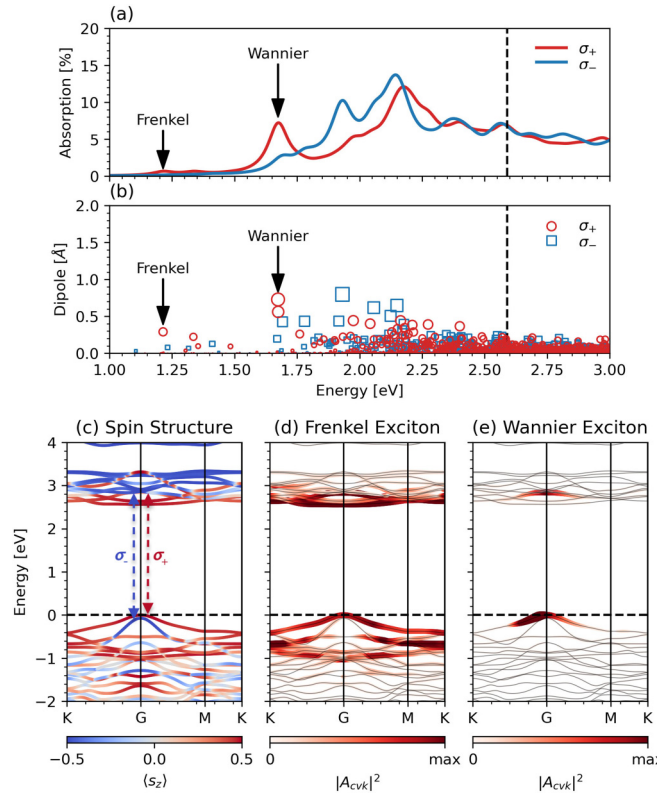

FIG. 2. (a) Absorption spectrum of a monolayer CrI_3 resolved in circular polarizations. The red profile corresponds to σ_+ polarized light and the blue profile to σ_- polarized light. Lorentzian broadening is taken equal to 40 meV. (b) Scatter plot of the exciton dipole moments resolved in circular polarizations. Main peaks are related to the Wannier-type excitons. (c) Spin-resolved band structure of CrI_3. The color code denotes the spin polarization $\langle s_z \rangle$ perpendicular to the monolayer plane, shown in the color bar below. Red (blue) dashed two-sided arrows show the dominant optical selection rule for σ_+ (σ_-) light polarization. (d) Band and momentum single-particle distribution of Frenkel-type excitons, as revealed by their strong delocalization in the momentum space. (e) Band and momentum single-particle distribution of Wannier-type excitons showing the strong localization in the momentum space.

Fig. 2(c) we highlight the band spin structure in the momentum space. The conduction and the valence bands are spin resolved, allowing for the visible spin resolution of the excitonic transitions. The main optical selection rules are shown in Fig. 2(c) by dashed two-sided arrows. We note that optical transitions between the bands with different spin polarizations are responsible for the emission of the photons of distinct polarizations.

In Figs. 2(d) and 2(e), we show a typical distribution of the single-particle contributions from various bands to Frenkel- and Wannier-type excitons. Frenkel excitons are characterized by a small radius, being of the order of magnitude of the lattice period. In the momentum space, they are formed by states originating from multiple bands and contain contributions from a wide momentum range. The high density of Frenkel-type excitons above 2 eV [Fig. 2(b)] leads to a blurred spectrum in this energy range, thus lowering the resolution of excitonic lines and reducing the effective Rabi splitting. We

thus concentrate on optical properties in the region $\leqslant 2$ eV, where Wannier-type excitons dominate the response, and peaks with huge Rabi splittings are clearly visible.

Wannier-type excitons have a much bigger Bohr radius and mostly contain the contributions from two well-defined single bands above and below the gap. An exciton at 1.7 eV is formed by a hole from the top of the upper valence band and an electron from the third conduction band, which have a negative effective mass at $\mathbf{k} = 0$ [see Fig. 2(e)], which is a unique feature of CrI_3 monolayers. Even though such a band arrangement does not match the most common configuration, for which the effective mass in the conduction band is positive, we can readily understand the origin of such a bound state qualitatively within the effective mass description of 2D excitons [54]. Considering the two-band model, the Hamiltonian of an electron-hole pair in the center-of-mass frame $\mathcal{H}_X$ reads

$$\mathcal{H}_X = -\frac{\hbar^2}{2\mu_{cv}}\nabla^2 - V(|\vec{r}|), \tag{1}$$

with $\vec{r}$ being the electron-hole relative position, μ_{cv} the reduced mass, and $V(|\vec{r}|)$ the attractive potential. The solutions of the Schrödinger equation with Hamiltonian (1) contain bound states when $\mu_{c,v} > 0$. If an electron has negative effective mass $m_c = -|m_c|$, the condition $\mu_{cv} = (m_v^{-1} - |m_c|^{-1})^{-1}$ leads to the constraint $|m_c| > m_v$ [55–57]. Electronic negative effective mass can lead to certain qualitative modifications of the nonlinear optical response governed by exciton-exciton interactions, but consideration of the related effects lies beyond the scope of the present Letter.

Polaritons in CrI_3 monolayers. We proceed to study the light-matter coupling in CrI_3 and its underlying polarization dependence. We consider a microcavity system with the CrI_3 layer embedded between cavity mirrors, as sketched in Fig. 1(b).

To study polarization-resolved photoluminescence, we assume that excitons are coupled to the single photonic mode, which has an antinode in the position where the monolayer is located, and use the Green's function approach.

The condition of placing the monolayer in the antinode comes from the need to maximize the light-matter coupling, and we choose the point where the electric field is the largest. As for exact cavity realization, we leave it open to experimental consideration [so far, a simple Fabry-Pérot geometry is shown in Fig. 1(b)].

The cavity photon propagator is expressed in the form of a 2×2 matrix $\hat{G}^{\rm ph}(\omega, \mathbf{q})$, describing two polarization components [58–60] with ω and $\mathbf{q}$ being the photon frequency and momentum, respectively. We account for the dressing of the cavity photons by excitonic quasiparticles in a nonperturbative way, and solve a Dyson-type equation for the renormalized photonic propagator $\hat{G}^{\rm ph}(\omega, \mathbf{q})$ [60,61] which is graphically shown in Fig. 3.

The renormalized photonic Green's function reads

$$\hat{G}^{\rm ph}(\omega, \mathbf{q}) = \frac{\hat{G}_0^{\rm ph}(\omega, \mathbf{q})}{1 - \hat{\Sigma}(\omega, \mathbf{q})\hat{G}_0^{\rm ph}(\omega, \mathbf{q})}, \tag{2}$$

where $\hat{\Sigma}(\omega, \mathbf{q})$ denotes the exciton self-energy obtained from the GW calculations. To get the dispersions of polaritonic modes, we look at the poles of the photon Green's function

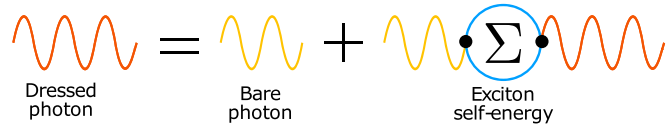

FIG. 3. Diagrammatic representation of the Dyson equation describing the light-matter coupling and resulting in Eq. (2). The polaritonic response is described by the dressed photon Green's function, corresponding to cavity photons that repeatedly interact with CrI_3 material excitations, described by the excitonic self-energy.

$\hat{G}^{\rm ph}$ dressed by material excitations. In the circular polarization basis the Green's function of a bare cavity photon reads

$$\hat{G}_0^{\rm ph}(\omega, \mathbf{q}) = \tfrac{1}{2}\left[\left(G_{\rm TE}^{\rm ph} + G_{\rm TM}^{\rm ph}\right)\hat{\sigma}_0 + \left(G_{\rm TE}^{\rm ph} - G_{\rm TM}^{\rm ph}\right)\hat{\sigma}_x\right], \tag{3}$$

where σ_0 is the identity matrix and the σ_x is the Pauli matrix and the bare photon Green's functions in transverse electric (TE) and transverse magnetic (TM) polarizations are

$$G_{\rm TE,TM}^{\rm ph} = \frac{2\omega_{\rm TE,TM}(\mathbf{q})}{\omega^2 - \omega_{\rm TE,TM}^2(\mathbf{q}) + 2i\gamma_c\omega_{\rm TE,TM}(\mathbf{q})}, \tag{4}$$

For the dispersion of cavity photons one can use the parabolic approximation $\omega_{\rm TE,TM}(\mathbf{q}) \approx \omega_0 + \hbar^2\mathbf{q}^2/2m_{\rm TE,TM}$. Here, ω_0 is the resonant frequency of a cavity at normal incidence, $m_{\rm TE,TM}$ are the effective masses of TE and TM polarized cavity photons, and γ_c is the broadening of the photonic line due to a finite transparency of the cavity mirrors.

We approximate the self-energy $\hat{\Sigma}(\omega, \mathbf{q})$ corresponding to excitonic transitions in both σ^+ and σ^- polarizations by the sum of the Lorentzians corresponding to individual excitons. Accounting for their polarization state, in matrix form the self-energy reads

$$\hat{\Sigma}(\omega, \mathbf{q}) = \frac{1}{2}\sum_j \frac{|\Omega_{j,\mathbf{0}}|^2}{\omega - \omega_j(\mathbf{q}) + i\gamma_j} \cdot [1 + s\hat{\sigma}_z], \tag{5}$$

where $s = \pm 1$ correspond to two opposite circular polarizations, $\Omega_{j,\mathbf{0}}$ are Rabi energies of the transitions, $\omega_j(\mathbf{q})$ are their resonant frequencies, and γ_j are nonradiative broadenings that depend on a sample quality.

Finally, the Rabi energies for excitonic transitions are calculated as [54,60]

$$\Omega_{\nu,\mathbf{q}} = \sqrt{\frac{2\omega_c(q)}{\hbar\varepsilon_0\varepsilon A}}\sum_{\mathbf{k}} d_{cv}(\mathbf{k}+\mathbf{q}, \mathbf{k})\langle\nu|\mathbf{k}+\mathbf{q}, \mathbf{k}\rangle, \tag{6}$$

where $d_{cv}(\mathbf{k}+\mathbf{q}, \mathbf{k})$ is a transition dipole matrix element, ε is a sample permittivity, and A is the sample area.

In Fig. 4, we show the polarization-resolved absorption spectra for the case of a cavity of 1 μm width in the two energy regions, 1.6–1.72 eV and 1.84–1.96 eV. Due to the ferromagnetic nature of CrI_3, the optical response of σ_+ and σ_- polarizations is qualitatively distinct. In the region of 1.6–1.72 eV, opposite circular polarizations show different Rabi splittings, as can be seen in Figs. 4(a) and 4(c), which leads to the significant polariton Zeeman splitting of the order of 10 meV. In the energy region 1.84–1.96 eV [Figs. 4(b) and 4(d)], the splitting between σ_+ and σ_- lower polaritons

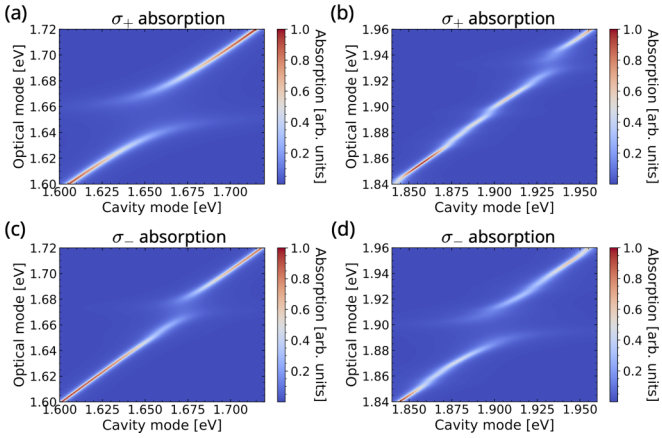

FIG. 4. Polarization-resolved CrI_3 polariton absorption in two different energy regions. [(a), (b)] σ_+ absorption profile revealing the presence of Rabi splittings of 32 and 14 meV around 1.66 and 1.93 eV, respectively. For the latter case the splitting is substantially reduced due to the high density of nondegenerate exciton modes. [(c), (d)] σ_- absorption profile revealing the presence of Rabi splittings of 16 and 34 meV for excitonic transitions at 1.67 and 1.90 eV, respectively.

becomes even stronger, which is due to the high density of excitonic states in this region and the corresponding redistribution of the oscillator strength.

We further highlight the two Rabi splittings (major $\sigma_\pm$ peaks) in Figs. 5(a) and 5(b), where we show the absorption spectra at different cavity detunings (curves are displaced vertically for clarity) in the two energy regions, where σ_+ and σ_- absorption dominates. The two peaks of each curve correspond to the lower (left peak) and upper (right peak) polariton branches for the leading polarization component. The minimal distance between the two peaks corresponds to the Rabi splitting and has the value of $\Omega = 32$ meV for σ_+ and $\Omega = 34$ meV for σ_-. Note that in the geometries with plasmonic cavities, one can expect that due to the reduction of the mode volume, the values of the Rabi splitting can be further increased [62]. Lower polariton branches corresponding to the two opposite circular polarizations as functions of cavity detunings corresponding to the excitonic peak located around 1.66 eV are shown in Fig. 5(c). The corresponding Zeeman splitting, defined as a difference in the energies of the two curves, is shown in Fig. 5(d). We find that it can reach the value of 20 meV.

Magnetopolaritons in CrI_3. The obtained values of the Rabi splitting for CrI_3-based systems exceed those characteristic to nonmagnetic TMD monolayers [63,64]. Moreover, we additionally report the presence of the giant polarization splitting of the polariton modes in the absence of an external magnetic field, which appears due to the ferromagnetic lattice ordering.

As an example, let us consider the region around the resonance located at 1.66 eV. One can see from Figs. 4(a) and 4(c)

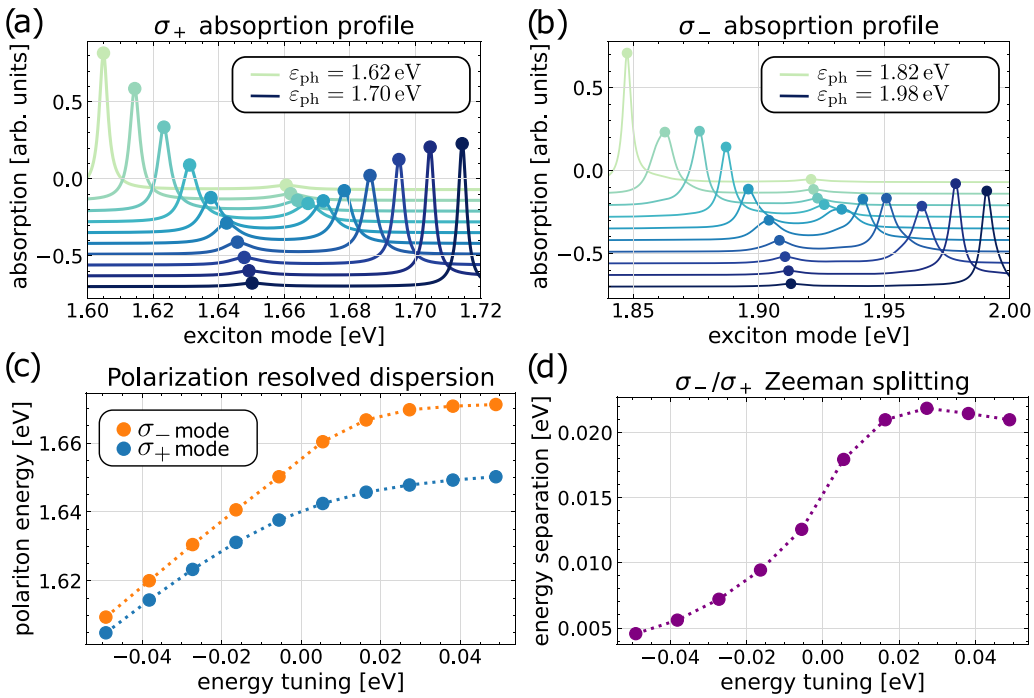

FIG. 5. [(a), (b)] Polariton absorption at different photon cavity detunings. (a) σ_+ absorption with Rabi splitting $\Omega = 32$ meV corresponding to the coupling of cavity photons with an excitonic transition at 1.66 eV. Different curves correspond to different energies of the cavity mode, which changes from 1.62 to 1.7 eV. (b) σ_- absorption with Rabi splitting $\Omega = 34$ meV corresponding to the coupling of cavity photons with an excitonic transition at 1.93 eV. Different curves correspond to different energies of the cavity mode, which changes from 1.84 up to 1.98 eV. (c) Lower polariton modes for σ_- (orange) and σ_+ (blue) polarizations, corresponding to the coupling of cavity photons with an excitonic transition at 1.66 eV. Plots are shown as a function of the detuning between exciton and cavity photon energies. (d) Zeeman splitting between σ_- and σ_+ lower polariton modes from (c). Due to the presence of ferromagnetic ordering, the corresponding characteristic value of about 15 meV at zero detuning.

that the corresponding excitons are strongly coupled with σ_+ polarized photons, which pushes the σ_+ lower polariton (LP_+) mode energy down to 1.64 eV. On the other hand, coupling with σ_- photons is much weaker, so that the σ_- lower polariton (LP_-) mode remains above the LP_+ [see Fig. 5(c)]. The distance between the two modes (polariton Zeeman splitting Δ_Z) becomes of the order 10–20 meV [Fig. 5(d)], which is about two orders of magnitude bigger than the record values reported both in nonmagnetic cavities based on conventional semiconductors [49,65,66] and TMD monolayers [67–70], and overcomes the values characteristic for magnetic semiconductor samples, where in sub-10-T magnetic fields one can reach $\Delta_Z \approx 5$ meV [71–73].

The possibility of breaking the symmetry between opposite circular polarizations lies at the core of magnetopolaritonics and allows spinoptronic applications, for instance, polariton Berry phase interferometry [74]. Large values of Zeeman splitting are also required for the realization of polariton Chern insulators [44,46,75], where topological edge states can be observed if Δ_Z exceeds the characteristic mode broadening [76]. Another exciting opportunity corresponds to the possibility of braiding the optical and spin excitations in the system [77,78]. Coherent magnon coupling to light has been proposed as a way for microwave-to-optical conversion devices, but the corresponding efficiency is usually small due to the weak coupling of magnons to light [79,80], and can be substantially increased in our system, where bright excitons can serve as the mediators [81].

Conclusions. In conclusion, we developed a microscopic theory to describe exciton polaritons in magnetic monolayers of CrI_3 placed in optical microcavities. We demonstrated that the presence of robust bright excitonic resonances leads to the formation of well-resolved polariton modes with values of the Rabi splitting up to 35 meV, which is comparable with values characteristic for TMD-based structures. Moreover, the presence of ferromagnetic ordering results in the huge values of the polariton Zeeman splittings of tens of meV, which makes CrI_3 monolayers excellent candidates for 2D magnetopolaritonics.

Acknowledgments. Y.Z. is grateful to HSE University Basic Research Program for financial support. S.C. and O.K. acknowledge the support from the U.K. EPSRC New Investigator Award under Agreement No. EP/V00171X/1, the NATO Science for Peace and Security Project No. NATO. S.P.S.MYP.G5860, and U.K. EPSRC New Horizons Grant No. EP/X017222/1. I.A.S. acknowledges support from the Icelandic Research Fund (project "Hybrid polaritonics"), Priority 2030 Federal Academic Leadership Program, and Ministry of Science and Education of Russian Federation (Agreement No. 075-15-2021-589).

[1] I. Carusotto and C. Ciuti, Rev. Mod. Phys. **85**, 299 (2013).
[2] G. Khitrova, H. Gibbs, M. Kira, S. W. Koch, and A. Scherer, Nat. Phys. **2**, 81 (2006).
[3] C. Weisbuch, M. Nishioka, A. Ishikawa, and Y. Arakawa, Phys. Rev. Lett. **69**, 3314 (1992).
[4] M. Zamfirescu, A. Kavokin, B. Gil, G. Malpuech, and M. Kaliteevski, Phys. Rev. B **65**, 161205(R) (2002).
[5] S. Christopoulos, G. Baldassarri Hoger von Högersthal, A. Grundy, P. G. Lagoudakis, A. V. Kavokin, J. J. Baumberg, G. Christmann, R. Butté, E. Feltin, J.-F. Carlin, and N. Grandjean, Phys. Rev. Lett. **98**, 126405 (2007).
[6] F. Li, L. Orosz, O. Kamoun, S. Bouchoule, C. Brimont, P. Disseix, T. Guillet, X. Lafosse, M. Leroux, J. Leymarie *et al.*, Phys. Rev. Lett. **110**, 196406 (2013).
[7] D. G. Lidzey, D. Bradley, M. Skolnick, T. Virgili, S. Walker, and D. Whittaker, Nature (London) **395**, 53 (1998).
[8] S. Kéna-Cohen and S. Forrest, Nat. Photonics **4**, 371 (2010).
[9] S. Kéna-Cohen, S. A. Maier, and D. D. Bradley, Adv. Opt. Mater. **1**, 827 (2013).
[10] J. D. Plumhof, T. Stöferle, L. Mai, U. Scherf, and R. F. Mahrt, Nat. Mater. **13**, 247 (2014).
[11] S. Betzold, M. Dusel, O. Kyriienko, C. P. Dietrich, S. Klembt, J. Ohmer, U. Fischer, I. A. Shelykh, C. Schneider, and S. Höfling, ACS Photonics **7**, 384 (2020).
[12] T. Yagafarov, D. Sannikov, A. Zasedatelev, K. Georgiou, A. Baranikov, O. Kyriienko, I. Shelykh, L. Gai, Z. Shen, D. Lidzey *et al.*, Commun. Phys. **3**, 18 (2020).
[13] G. Lanty, A. Brehier, R. Parashkov, J.-S. Lauret, and E. Deleporte, New J. Phys. **10**, 065007 (2008).
[14] R. Su, C. Diederichs, J. Wang, T. C. Liew, J. Zhao, S. Liu, W. Xu, Z. Chen, and Q. Xiong, Nano Lett. **17**, 3982 (2017).
[15] A. Fieramosca, L. Polimeno, V. Ardizzone, L. De Marco, M. Pugliese, V. Maiorano, M. De Giorgi, L. Dominici, G. Gigli, D. Gerace *et al.*, Sci. Adv. **5**, eaav9967 (2019).
[16] L. Polimeno, A. Fieramosca, G. Lerario, M. Cinquino, M. De Giorgi, D. Ballarini, F. Todisco, L. Dominici, V. Ardizzone, M. Pugliese *et al.*, Adv. Opt. Mater. **8**, 2000176 (2020).
[17] R. Su, S. Ghosh, J. Wang, S. Liu, C. Diederichs, T. C. Liew, and Q. Xiong, Nat. Phys. **16**, 301 (2020).
[18] A. Graf, L. Tropf, Y. Zakharko, J. Zaumseil, and M. C. Gather, Nat. Commun. **7**, 13078 (2016).
[19] C. Möhl, A. Graf, F. J. Berger, J. Lüttgens, Y. Zakharko, V. Lumsargis, M. C. Gather, and J. Zaumseil, ACS Photonics **5**, 2074 (2018).
[20] V. A. Shahnazaryan, V. A. Saroka, I. A. Shelykh, W. L. Barnes, and M. E. Portnoi, ACS Photonics **6**, 904 (2019).
[21] A. Splendiani, L. Sun, Y. Zhang, T. Li, J. Kim, C.-Y. Chim, G. Galli, and F. Wang, Nano Lett. **10**, 1271 (2010).
[22] A. Chernikov, T. C. Berkelbach, H. M. Hill, A. Rigosi, Y. Li, B. Aslan, D. R. Reichman, M. S. Hybertsen, and T. F. Heinz, Phys. Rev. Lett. **113**, 076802 (2014).
[23] S. Schwarz, S. Dufferwiel, P. Walker, F. Withers, A. Trichet, M. Sich, F. Li, E. Chekhovich, D. Borisenko, N. N. Kolesnikov *et al.*, Nano Lett. **14**, 7003 (2014).
[24] X. Liu, T. Galfsky, Z. Sun, F. Xia, E.-c. Lin, Y.-H. Lee, S. Kéna-Cohen, and V. M. Menon, Nat. Photonics **9**, 30 (2015).
[25] S. Dufferwiel, S. Schwarz, F. Withers, A. Trichet, F. Li, M. Sich, D. Pozo-Zamudio, C. Clark, A. Nalitov, D. Solnyshkov *et al.*, Nat. Commun. **6**, 8579 (2015).
[26] N. Lundt, A. Maryński, E. Cherotchenko, A. Pant, X. Fan, S. Tongay, G. Sęk, A. V. Kavokin, S. Höfling, and C. Schneider, 2D Mater. **4**, 015006 (2016).

[27] C. Schneider, M. M. Glazov, T. Korn *et al.*, Nat. Commun. **9**, 2695 (2018).

[28] P. Gonçalves, N. Stenger, J. D. Cox, N. A. Mortensen, and S. Xiao, Adv. Opt. Mater. **8**, 1901473 (2020).

[29] P. Steinleitner, P. Merkl, P. Nagler, J. Mornhinweg, C. Schüller, T. Korn, A. Chernikov, and R. Huber, Nano Lett. **17**, 1455 (2017).

[30] G. Wang, A. Chernikov, M. M. Glazov, T. F. Heinz, X. Marie, T. Amand, and B. Urbaszek, Rev. Mod. Phys. **90**, 021001 (2018).

[31] M. Wu, Z. Li, T. Cao, and S. G. Louie, Nat. Commun. **10**, 2371 (2019).

[32] H. Deng, H. Haug, and Y. Yamamoto, Rev. Mod. Phys. **82**, 1489 (2010).

[33] K. S. Burch, D. Mandrus, and J.-G. Park, Nature (London) **563**, 47 (2018).

[34] C. Gong and X. Zhang, Science **363**, eaav4450 (2019).

[35] B. Huang, G. Clark, E. Navarro-Moratalla, D. R. Klein, R. Cheng, K. L. Seyler, D. Zhong, E. Schmidgall, M. A. McGuire, D. H. Cobden *et al.*, Nature (London) **546**, 270 (2017).

[36] F. Zheng, J. Zhao, Z. Liu, M. Li, M. Zhou, S. Zhang, and P. Zhang, Nanoscale **10**, 14298 (2018).

[37] I. Kashin, V. Mazurenko, M. Katsnelson, and A. Rudenko, 2D Mater. **7**, 025036 (2020).

[38] G. Cheng, M. M. Rahman, A. L. Allcca *et al.*, Nat Electron **6**, 434 (2023).

[39] Z. Liu, Y. Han, Y. Ren, Q. Niu, and Z. Qiao, Phys. Rev. B **104**, L121403 (2021).

[40] Y. O. Kvashnin, A. N. Rudenko, P. Thunström, M. Rösner, and M. I. Katsnelson, Phys. Rev. B **105**, 205124 (2022).

[41] K. L. Seyler, D. Zhong, D. R. Klein, S. Gao, X. Zhang, B. Huang, E. Navarro-Moratalla, L. Yang, D. H. Cobden, M. A. McGuire *et al.*, Nat. Phys. **14**, 277 (2018).

[42] A. A. Pervishko, D. Yudin, V. K. Gudelli, A. Delin, O. Eriksson, and G.-Y. Guo, Opt. Express **28**, 29155 (2020).

[43] P. Zhang, T.-F. Chung, Q. Li, S. Wang, Q. Wang, W. L. B. Huey, S. Yang, J. E. Goldberger, J. Yao, and X. Zhang, Nat. Mater. **21**, 1373 (2022).

[44] A. V. Nalitov, D. D. Solnyshkov, and G. Malpuech, Phys. Rev. Lett. **114**, 116401 (2015).

[45] T. Karzig, C.-E. Bardyn, N. H. Lindner, and G. Refael, Phys. Rev. X **5**, 031001 (2015).

[46] S. Klembt, T. Harder, O. Egorov, K. Winkler, R. Ge, M. Bandres, M. Emmerling, L. Worschech, T. Liew, M. Segev *et al.*, Nature (London) **562**, 552 (2018).

[47] A. V. Yulin, A. V. Nalitov, and I. A. Shelykh, Phys. Rev. B **101**, 104308 (2020).

[48] Y. G. Rubo, A. Kavokin, and I. Shelykh, Phys. Lett. A **358**, 227 (2006).

[49] P. Walker, T. C. H. Liew, D. Sarkar, M. Durska, A. P. D. Love, M. S. Skolnick, J. S. Roberts, I. A. Shelykh, A. V. Kavokin, and D. N. Krizhanovskii, Phys. Rev. Lett. **106**, 257401 (2011).

[50] J. R. Schaibley, H. Yu, G. Clark, P. Rivera, J. S. Ross, K. L. Seyler, W. Yao, and X. Xu, Nat. Rev. Mater. **1**, 16055 (2016).

[51] F. Dirnberger, R. Bushati, B. Datta, A. Kumar, A. H. MacDonald, E. Baldini, and V. M. Menon, Nat. Nanotechnol. **17**, 1060 (2022).

[52] See Supplemental material at http://link.aps.org/supplemental/10.1103/PhysRevB.108.L161402 for computational details concerning the DFT calculations and numerical solution of the Bethe-Salpeter equation, which contains Refs. [82–90].

[53] T. Olsen, Phys. Rev. Lett. **127**, 166402 (2021).

[54] H. Haug and S. W. Koch, *Quantum Theory of the Optical and Electronic Properties of Semiconductors* (World Scientific, Singapore, 2009).

[55] K.-Q. Lin, S. Bange, and J. M. Lupton, Nat. Phys. **15**, 242 (2019).

[56] K.-Q. Lin, C. S. Ong, S. Bange, P. E. F. Junior, B. Peng, J. D. Ziegler, J. Zipfel, C. Bäuml, N. Paradiso, K. Watanabe, T. Taniguchi, C. Strunk, B. Monserrat, J. Fabian, A. Chernikov, D. Y. Qiu, S. G. Louie, and J. M. Lupton, Nat. Commun. **12**, 5500 (2021).

[57] K.-Q. Lin, P. E. Faria Junior, J. M. Bauer, B. Peng, B. Monserrat, M. Gmitra, J. Fabian, S. Bange, and J. M. Lupton, Nat. Commun. **12**, 1553 (2021).

[58] O. Kyriienko and I. A. Shelykh, J. Nanophotonics **6**, 061804 (2012).

[59] O. Kyriienko and I. A. Shelykh, Phys. Rev. B **87**, 075446 (2013).

[60] Y. V. Zhumagulov, S. Chiavazzo, D. R. Gulevich, V. Perebeinos, I. A. Shelykh, and O. Kyriienko, npj Comput. Mater. **8**, 92 (2022).

[61] K. B. Arnardottir, O. Kyriienko, M. E. Portnoi, and I. A. Shelykh, Phys. Rev. B **87**, 125408 (2013).

[62] J. Cuadra, D. G. Baranov, M. Wersäll, R. Verre, T. J. Antosiewicz, and T. Shegai, Nano Lett. **18**, 1777 (2018).

[63] Y. Chen, S. Miao, T. Wang, D. Zhong, A. Saxena, C. Chow, J. Whitehead, D. Gerace, X. Xu, S.-F. Shi *et al.*, Nano Lett. **20**, 5292 (2020).

[64] M.-E. Kleemann, R. Chikkaraddy, E. M. Alexeev, D. Kos, C. Carnegie, W. Deacon, A. C. De Pury, C. Große, B. De Nijs, J. Mertens *et al.*, Nat. Commun. **8**, 1296 (2017).

[65] B. Piętka, D. Zygmunt, M. Król, M. R. Molas, A. A. L. Nicolet, F. Morier-Genoud, J. Szczytko, J. Łusakowski, P. Zięba, I. Tralle, P. Stępnicki, M. Matuszewski, M. Potemski, and B. Deveaud, Phys. Rev. B **91**, 075309 (2015).

[66] A. Rahimi-Iman, C. Schneider, J. Fischer, S. Holzinger, M. Amthor, S. Höfling, S. Reitzenstein, L. Worschech, M. Kamp, and A. Forchel, Phys. Rev. B **84**, 165325 (2011).

[67] N. Lundt, M. Klaas, E. Sedov, M. Waldherr, H. Knopf, M. Blei, S. Tongay, S. Klembt, T. Taniguchi, K. Watanabe, U. Schulz, A. Kavokin, S. Höfling, F. Eilenberger, and C. Schneider, Phys. Rev. B **100**, 121303(R) (2019).

[68] A. Srivastava, M. Sidler, A. V. Allain, D. S. Lembke, A. Kis, and A. Imamoğlu, Nat. Phys. **11**, 141 (2015).

[69] S. Dufferwiel, T. P. Lyons, D. D. Solnyshkov, A. A. P. Trichet, F. Withers, S. Schwarz, G. Malpuech, J. M. Smith, K. S. Novoselov, M. S. Skolnick, D. N. Krizhanovskii, and A. I. Tartakovskii, Nat. Photonics **11**, 497 (2017).

[70] S. Dufferwiel, T. P. Lyons, D. D. Solnyshkov, A. A. P. Trichet, A. Catanzaro, F. Withers, G. Malpuech, J. M. Smith, K. S. Novoselov, M. S. Skolnick, D. N. Krizhanovskii, and A. I. Tartakovskii, Nat. Commun. **9**, 4797 (2018).

[71] R. Mirek, M. Król, K. Lekenta, J.-G. Rousset, M. Nawrocki, M. Kulczykowski, M. Matuszewski, J. Szczytko, W. Pacuski, and B. Piętka, Phys. Rev. B **95**, 085429 (2017).

[72] J.-G. Rousset, B. Piętka, M. Król, R. Mirek, K. Lekenta, J. Szczytko, W. Pacuski, and M. Nawrocki, Phys. Rev. B **96**, 125403 (2017).

[73] A. Brunetti, M. Vladimirova, D. Scalbert, R. André, D. Solnyshkov, G. Malpuech, I. A. Shelykh, and A. V. Kavokin, Phys. Rev. B **73**, 205337 (2006).
[74] I. A. Shelykh, G. Pavlovic, D. D. Solnyshkov, and G. Malpuech, Phys. Rev. Lett. **102**, 046407 (2009).
[75] C.-E. Bardyn, T. Karzig, G. Refael, and T. C. H. Liew, Phys. Rev. B **91**, 161413(R) (2015).
[76] D. D. Solnyshkov, G. Malpuech, P. St-Jean, S. Ravets, J. Bloch, and A. Amo, Opt. Mater. Express **11**, 1119 (2021).
[77] J. Cenker, B. Huang, N. Suri, P. Thijssen, A. Miller, T. Song, T. Taniguchi, K. Watanabe, M. A. McGuire, D. Xiao, and X. Xu, Nat. Phys. **17**, 20 (2021).
[78] L. Chen, J.-H. Chung, B. Gao, T. Chen, M. B. Stone, A. I. Kolesnikov, Q. Huang, and P. Dai, Phys. Rev. X **8**, 041028 (2018).
[79] A. Osada, R. Hisatomi, A. Noguchi, Y. Tabuchi, R. Yamazaki, K. Usami, M. Sadgrove, R. Yalla, M. Nomura, and Y. Nakamura, Phys. Rev. Lett. **116**, 223601 (2016).
[80] A. Osada, A. Gloppe, R. Hisatomi, A. Noguchi, R. Yamazaki, M. Nomura, Y. Nakamura, and K. Usami, Phys. Rev. Lett. **120**, 133602 (2018).
[81] A. Kudlis, I. Iorsh, and I. A. Shelykh, Phys. Rev. B **104**, L020412 (2021).
[82] I. C. Gerber, E. Courtade, S. Shree, C. Robert, T. Taniguchi, K. Watanabe, A. Balocchi, P. Renucci, D. Lagarde, X. Marie, and B. Urbaszek, Phys. Rev. B **99**, 035443 (2019).
[83] M. Z. Mayers, T. C. Berkelbach, M. S. Hybertsen, and D. R. Reichman, Phys. Rev. B **92**, 161404(R) (2015).
[84] K. A. Velizhanin and A. Saxena, Phys. Rev. B **92**, 195305 (2015).
[85] J. J. Mortensen, L. B. Hansen, and K. W. Jacobsen, Phys. Rev. B **71**, 035109 (2005).
[86] J. Enkovaara, C. Rostgaard, J. J. Mortensen, J. Chen, M. Dułak, L. Ferrighi, J. Gavnholt, C. Glinsvad, V. Haikola, H. A. Hansen, H. H. Kristoffersen, M. Kuisma, A. H. Larsen, L. Lehtovaara, M. Ljungberg, O. Lopez-Acevedo, P. G. Moses, J. Ojanen, T. Olsen, V. Petzold *et al.*, J. Phys.: Condens. Matter **22**, 253202 (2010).
[87] T. Olsen, Phys. Rev. B **94**, 235106 (2016).
[88] M. Rohlfing and S. G. Louie, Phys. Rev. B **62**, 4927 (2000).
[89] J. Yan, J. J. Mortensen, K. W. Jacobsen, and K. S. Thygesen, Phys. Rev. B **83**, 245122 (2011).
[90] F. Hüser, T. Olsen, and K. S. Thygesen, Phys. Rev. B **88**, 245309 (2013).